



THE UNIVERSITY *of* EDINBURGH

Edinburgh Research Explorer

Sensitivity analysis of an unsteady char particle combustion

Citation for published version:

Hassan, A, Sayadi, T, Le Chenadec, V & Attili, A 2021, 'Sensitivity analysis of an unsteady char particle combustion', *Fuel*, vol. 287, 119738. <https://doi.org/10.1016/j.fuel.2020.119738>

Digital Object Identifier (DOI):

[10.1016/j.fuel.2020.119738](https://doi.org/10.1016/j.fuel.2020.119738)

Link:

[Link to publication record in Edinburgh Research Explorer](#)

Document Version:

Peer reviewed version

Published In:

Fuel

General rights

Copyright for the publications made accessible via the Edinburgh Research Explorer is retained by the author(s) and / or other copyright owners and it is a condition of accessing these publications that users recognise and abide by the legal requirements associated with these rights.

Take down policy

The University of Edinburgh has made every reasonable effort to ensure that Edinburgh Research Explorer content complies with UK legislation. If you believe that the public display of this file breaches copyright please contact openaccess@ed.ac.uk providing details, and we will remove access to the work immediately and investigate your claim.



Sensitivity analysis of an unsteady char particle combustion

Ahmed Hassan · Taraneh Sayadi ·
Vincent Le Chenadec · Antonio Attili

Received: date / Accepted: date

Abstract Simulations of unsteady char particle combustion rely on various models that are necessary in order to correctly predict the governing flow and combustion processes. These models, in turn, rely on model parameters, which are determined by experiments or small scale simulations and contain a certain level of uncertainty. It is therefore, essential to correctly determine the sensitivities of quantities of interest measured using such simulations, with respect to the existing parameters. In this study, a discrete adjoint algorithm is employed to extract sensitivities of various quantities of interest with respect to physical and model parameters. This adjoint framework bears a great advantage in cases where a large input space is analyzed, since a single forward and backward sweep provides sensitivity information with respect to all parameters of interest. Sensitivities are extracted for relevant quantities of interest, such as burning rate and particle temperature, and are then compared as free stream composition changes from air to oxy atmosphere. The evolution of sensitivities in time is shown to be dependent on the selected quantity of interest. Model sensitivities with respect to heterogeneous reaction parameters (oxidation of carbon, in particular) are shown to be the highest, whereas the sensitivities with respect to free stream composition are shown to be significantly lower.

A. Hassan

Institute of Combustion Technology, RWTH-Aachen University, Aachen, Germany
E-mail: a.hassan@itv.rwth-aachen.de

T. Sayadi

Jean le Rond d'Alembert Institute, CNRS/Sorbonne University, Paris, France
Institute of Combustion Technology, RWTH-Aachen University, Aachen, Germany

V. Le Chenadec

Multiscale Modelling and Simulation Laboratory, Paris – Est University, France

A. Attili

Institute of Combustion Technology, RWTH-Aachen University, Aachen, Germany
Institute for Multiscale Thermofluids, School of Engineering, University of Edinburgh,
United Kingdom

Keywords Unsteady char burnout · Sensitivity analysis · Computational fluid dynamics

1 Introduction

Energy conversion devices burn fuel in spray (liquid fuel) or pulverised (solid fuel) form. Understanding the details of the combustion process on the scale of droplets/particles is therefore essential in correctly predicting the behaviour of the system on the larger scale, for example, that of the full-sized burner. Coal particle combustion, in particular, is composed of devolatilisation, followed by the resulting char burnout. Volatiles consist of light gases and tars, and during the faster devolatilisation process, the species in the light fraction are partially oxidised. While some models consider the overlap of volatiles and char combustion [2], it is common to separate the two processes and assume that char burns only after volatile evolution has ceased [1], which for coal particles with less volatile matter is an acceptable assumption. This is the strategy adopted in this study.

Early analytical and numerical investigations of char burnout focused entirely on the steady state solution. Analytical studies, such as those carried out by Matalon [28] and Makino [27], provide insight towards asymptotic behaviour of char burnout in the frozen limit. On the other hand, axisymmetric [25,26] and two-dimensional [14,16,20] simulations present the dynamics in the intermediate regime, where a flame is present in the gas-phase. The high complexity of the pulverised and fluidised bed coal combustion, however, has motivated the analysis of unsteady combustion of single coal particles. In this context, both one-dimensional (spherically symmetric) [22,38] and two-dimensional [21,11] simulations of the combustion process have been performed.

Regardless of the fidelity of the simulations, a certain level of modelling is usually employed in order to correctly capture the combustion process. The most conventional models used to simulate coal particle combustion are single film [30,10], double film [37], and continuous film [15] models. These models are mostly developed in one-dimensional settings and in the steady state limit. The fidelity of the model can be increased by considering ever more complex gas and particle-phase chemistry [29]. These models generally rely on many parameters in order to approximate the physical problem. These parameters are determined using experiments or small-scale simulations, and when used in large-scale simulations, can result in unreliable predictions, due to the level of uncertainties they contain. Since the simulations are generally performed to estimate a desired output quantity (final solution, or quantity of interest such as the burning rate of particles or the global heat release in the domain), it is of great importance to determine the sensitivity of the desired output to the model parameters. This information can serve to either improve the model or provide insight towards sensitive operating points in the modelled simulation. In practice, most of the sensitivity information is extracted in small-scale

simulations, focusing solely on the kinetics, and therefore ignoring the effect of the underlying multi-dimensional flow [34,5]. This is usually due to the fact that extracting the Jacobian (gradient) of the full system, including the coupled hydrodynamic and reactive equations, using conventional approaches, can become very expensive and in many real scale applications infeasible.

Most common methods in extracting the gradient information are analytical or use finite differences, neither of which is suited to complex flow configurations. Adjoint methods present a suitable alternative, since they allow the computation of the gradient at a cost comparable to a single function evaluation [13]. The benefit of this formalism lies in the low dimensionality of the output (performance) space, independent of the dimensionality of the input (parameter) space. Adjoint methods are therefore very effective in situations where multiple parameters are present, which is the case in this study.

The use of the adjoint method for design and optimization has been an active area of research pioneered by Pironneau [31], and has been applied extensively in the fields of acoustics and thermo-acoustics [19,24]. These areas provide suitable ground for adjoint-based methods, which are inherently linear, since they too are dominated by linear dynamics. Recently, non-linear problems have also been tackled [36,32,12]. However, few applications to more complex flow scenarios, such as reactive flows, have been documented. In the case of reactive flows, adjoint-based methods have been employed for adaptive mesh refinement in steady-state Reynolds Averaged Navier-Stokes (RANS) simulations [8]. As far as detailed simulations are concerned, Braman *et al.* [4] have investigated the applicability of adjoint-based techniques in one- and two-dimensional laminar flow configurations, where the hydrodynamics are decoupled from the reactive equations. Recently, Lemke *et al.* [23] have also explored the applicability of such techniques in the zero-dimensional case of a homogeneous constant volume reactor, to study the sensitivity of the ignition delay time with respect to the combustion model parameters. The unsteady and non-linear governing equations used in the present study, which couple combustion and hydrodynamics, brings new challenges to the application of adjoint-based techniques.

Traditionally, adjoint equations are derived from the continuous equations by applying a variational principle to the unconstrained optimization problem and setting the first variations with respect to all independent variables to zero. This results in governing equations for the direct (primal) and for the adjoint (dual) variables, together with appropriate boundary and initial conditions as well as optimality conditions, which subsequently have to be discretized and solved [18,3,41]. As the dimensionality and complexity of the governing equations increase, the applicability of this strategy becomes infeasible. Alternatively, the spatially discretized equations (e.g. resulting from the application of the method of lines) can be used and processed by automatic (or algorithmic) differentiation (AD) software to produce the associated adjoint code [33]. In this study, the focus is placed on discrete adjoint algorithms. In particular, the applicability of such algorithms is examined in extracting

sensitivities with respect to the model/physical parameters of unsteady char combustion.

The paper is structured as follows. Section 2, describes the governing equations and the combustion models used to capture the combustion processes on the particle surface and in the gas-phase. Section 3, presents the resulting equations from the forward sensitivity methodology, followed by the numerical strategy for solving the non-linear and linear systems of equations, discussed in section 4. The results are then discussed in section 5, followed by summary and conclusions in section 6.

2 Governing equations

The equations governing an axisymmetric unsteady single char particle combustion in the low Mach number limit (these assumptions eliminate the need for the momentum equation), are given below;

$$\frac{\partial \rho}{\partial t} + \frac{1}{r^\alpha} \frac{\partial}{\partial r} (\rho r^\alpha u) = 0, \quad (1)$$

$$\frac{\partial \rho Y_i}{\partial t} + \frac{1}{r^\alpha} \frac{\partial}{\partial r} \left[\rho r^\alpha \left(u Y_i - D_i \frac{\partial Y_i}{\partial r} \right) \right] - \omega_i = 0, \quad (2)$$

$$\frac{\partial \rho c_p T}{\partial t} + \frac{1}{r^\alpha} \frac{\partial}{\partial r} \left[\rho r^\alpha \left(u c_p T - \lambda \frac{\partial T}{\partial r} \right) \right] + \sum h_i \omega_i = 0, \quad (3)$$

where Fick's law of diffusion and Fourier's law of heat conduction are used, t and r are independent coordinates, and α is a parameter depending on the spatial coordinate system r . For $\alpha = 0$, the above equations are written in Cartesian coordinates, $\alpha = 1$ in cylindrical coordinates, and $\alpha = 2$ in spherical coordinates. The dependent variables (Y_i), ρ , u , and T represent the mass fractions, density, radial velocity, and temperature fields, respectively. The parameters λ , c_p , and D_i are the gas thermal conductivity, the gas heat capacity at constant pressure, and species diffusivities, which are computed assuming unity Lewis number. The species are numbered as follows: $(Y_i) = (Y_{\text{CO}}, Y_{\text{O}_2}, Y_{\text{CO}_2}, Y_{\text{N}_2})$. The governing equations are transformed from the physical coordinates (r, t) to a mass-based coordinate system (ψ, τ) . This transformation is not necessary, but it presents a couple of advantages. First, the velocity disappears from the transport equations, which also eliminates the need for an initial velocity profile. Second, the domain size is automatically scaled. It should be noted, however, that the applicability of the adjoint-based algorithm is independent of this choice. This transformation is achieved using the following equations;

$$\frac{\partial}{\partial r} = \rho r^\alpha \frac{\partial}{\partial \psi}, \quad (4)$$

for the spatial and

$$\frac{\partial}{\partial t} = \frac{\partial}{\partial \tau} - \rho r_0^\alpha u_r \frac{\partial}{\partial \psi} + \dot{m}_0^\alpha \frac{\partial}{\partial \psi}, \quad (5)$$

for the temporal derivatives. In these equations, $\dot{m}_0^\alpha = \dot{M}_w/C_\alpha$ represents the mass flux at the surface of the particle (\dot{M}_w) per unit surface area (C_α) and r_0 is the particle radius. $C_2 = 4\pi$ in the spherical case, $C_1 = 2\pi H$ (H denoting the height) in the cylindrical case, and $C_0 = HW$ (H and W denoting the height and width) in the Cartesian case. Using the identified parameters with the assumption of unity Lewis number, the equations governing the evolution of species and energy are transformed as follows;

$$\frac{\partial Y_i}{\partial \tau} + \dot{m}_0^\alpha \frac{\partial Y_i}{\partial \psi} - \frac{\lambda}{c_p} \frac{\partial}{\partial \psi} \left(\rho r^{2\alpha} \frac{\partial Y_i}{\partial \psi} \right) - \frac{\omega_i}{\rho} = 0, \quad (6)$$

$$\frac{\partial T}{\partial \tau} + \dot{m}_0^\alpha \frac{\partial T}{\partial \psi} - \frac{\lambda}{c_p} \frac{\partial}{\partial \psi} \left(\rho r^{2\alpha} \frac{\partial T}{\partial \psi} \right) + \frac{1}{\rho c_p} \sum h_i \omega_i = 0. \quad (7)$$

Finally, the mass conservation equation is satisfied by the following equation,

$$\frac{\partial r}{\partial \psi} = \frac{1}{\rho r^\alpha}. \quad (8)$$

This equation is otherwise referred to as the mapping equation, used to express the original coordinate r as a function of the mass-based coordinate ψ .

2.1 Boundary conditions

The boundary conditions at the surface of the particle are extracted from the species conservation equation, that expresses the balance between convective and diffusive transport on the one hand, and heterogeneous reactions on the other hand. In (ψ, τ) coordinate system, the resulting Robin boundary conditions read,

$$\dot{M}_w Y_{i,w} - C_\alpha \rho r_0^{2\alpha} \frac{\lambda}{c_p} \frac{\partial Y_i}{\partial \psi} \Big|_w - \omega_{i,s} = 0. \quad (9)$$

Subscript w identifies variables calculated at the surface of the particle. The particle burning rate, directly connected to the mass flow rate at the surface, can be computed as follows,

$$\dot{M}_w = \dot{m}_{c,1} + \dot{m}_{c,2}, \quad (10)$$

where $\dot{m}_{c,1}$ and $\dot{m}_{c,2}$ are the char reaction rate due to direct oxidation and gasification, respectively (described in detail in section 2.2.1). Assuming a homogeneous temperature profile in the particle, a Dirichlet boundary condition is used for the gas phase temperature at the particle surface, resulting in,

$$T_s^g = T_p. \quad (11)$$

This algebraic equation requires an initial condition for completeness, leading to,

$$\psi(r = r_0) = 0. \quad (12)$$

Satisfying energy conservation in a control volume surrounding the particle surface results in the evolution equation for the particle temperature, given as,

$$M_p c_s \frac{\partial T_p}{\partial \tau} - C_\alpha \rho r_0^{2\alpha} \lambda_w \frac{\partial T}{\partial \psi} - (\dot{m}_{c,1} h_{c,1} + \dot{m}_{c,2} h_{c,2}) = 0, \quad (13)$$

where the enthalpy of the two surface reactions are, $h_1 = \frac{117 \times 10^3}{W_C} \text{J/kg}_C$ and $h_2 = \frac{-172 \times 10^3}{W_C} \text{J/kg}_C$, respectively, as proposed by Tirado *et al.* [40]. M_p represents the particle mass, and c_s the specific heat capacity of char. λ_w is the heat conductivity, determining heat conduction at the surface of the particle. In this study, the particle is assumed to have a homogeneous temperature on the surface and inside, therefore, the only heat conduction is from the gas to the particle, resulting in $\lambda_w = \lambda_g$.

Finally, the boundary conditions in the far-field are expressed explicitly as Dirichlet boundary conditions:

$$Y_i(\tau, \psi \rightarrow \infty) = Y_i^\infty, \quad (14)$$

$$T(\tau, \psi \rightarrow \infty) = T^\infty. \quad (15)$$

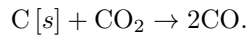
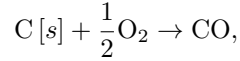
For the purpose of this study, the particle is considered to be spherical and α is therefore set to 2.

2.2 Chemical models

The above equations are finally closed by selecting a specific kinetic model describing the heterogeneous and homogeneous reactions, and resulting in the respective reaction rates, defining ω_i 's, $\dot{m}_{c,1}$, and $\dot{m}_{c,2}$.

2.2.1 Heterogeneous reactions

The combustion process on the surface of the particle is approximated by the following heterogeneous reactions (referred to as direct and indirect oxidation, respectively),



The reaction rates are expressed as a function of the partial pressure of the gaseous species at the surface, given by;

$$\omega_{c,1} = A_1 P_1^{n_1} \exp\left(\frac{-E_1}{RT_p}\right), \quad (16)$$

$$\omega_{c,2} = A_2 P_2^{n_2} \exp\left(\frac{-E_2}{RT_p}\right), \quad (17)$$

where $A_1 = 0.095 \text{kg/m}^2/\text{s}/\text{Pa}$, $E_1 = 108 \text{kJ/mol}_C$, $A_2 = 7.55 \text{kg/m}^2/\text{s}/\text{Pa}^{0.45}$, $E_2 = 148.5 \text{kJ/mol}_C$, $n_1 = 1$, $n_2 = 0.45$ and P_i is the partial pressure of species

$i \in \{\text{O}_2, \text{CO}_2\}$. Detailed description of the parameters can be found in [39]. The reaction rate of other species at the surface can be computed from the char reaction rate by,

$$\omega_{i,s} = X_i \omega_{c,1} + Z_i \omega_{c,2}, \quad (18)$$

where,

$$(X_i) = (W_{\text{CO}}/W_C, -W_{\text{O}_2}/2W_C, 0, 0),$$

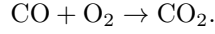
and

$$(Z_i) = (2W_{\text{CO}}/W_C, 0, -W_{\text{CO}_2}/W_C, 0).$$

Finally, W_C denotes the molecular weight of carbon and W_{O_2} the molecular weight of oxygen.

2.2.2 Homogeneous reaction

In this study, a single global reaction, oxidation of carbon monoxide, governs the gas phase chemistry,



Therefore, the source terms appearing on the right-hand-side of species equation 6 are expressed using the reaction rate of the carbon monoxide oxidation reaction, given as,

$$\omega_i = \nu_i \omega_{\text{CO}}, \quad (19)$$

where ν_i represents the mass-based stoichiometric ratio between the species i and the carbon monoxide. The reaction rate of CO can be modelled, as proposed by Tirado *et al.* [40], by

$$\omega_{\text{CO}} = \frac{-K \rho^2 Y_{\text{H}_2\text{O}}^{0.5}}{W_{\text{CO}} W_{\text{O}_2}^{0.5} W_{\text{H}_2\text{O}}^{0.5}} Y_{\text{CO}} Y_{\text{O}_2}^{0.5} \exp\left(\frac{-E_g}{RT}\right), \quad (20)$$

where, $K = 1.23 \times 10^8$, $E_g = 125400$ kJ/mole_C, $Y_{\text{H}_2\text{O}} = 10^{-3}$ and W_i denotes the molecular weight of the i^{th} species.

In this study, following the model proposed by Matalon [28], mass fraction of water is assumed to be small, and its variation inside the domain is considered negligible. Further analysis to determine the effect of water on the overall sensitivities will be the subject of future research. Assuming constant thermodynamic parameters, the source term of the energy equation can be defined as follows,

$$\omega \sum W_i h_i^0 (\nu_i'' - \nu_i') = \omega_{\text{CO}_2} \frac{W_{\text{CO}}}{W_{\text{CO}_2}} H_{\text{CO}} + \omega_{\text{CO}_2} H_{\text{CO}_2}, \quad (21)$$

where $H_{\text{CO}} = 110.53/W_{\text{CO}}$ kJ/kg and $H_{\text{CO}_2} = 393.474/W_{\text{CO}_2}$ kJ/kg. W_{CO} and W_{CO_2} denote the molecular weight of carbon monoxide and carbon dioxide respectively.

3 Gradient computation

Sensitivity is, in effect, the rate of change in a measured quantity of interest (QoI) with respect to a parameter or variable. It is a signed quantity that signifies whether a change in the parameter will lead to an increase or decrease in the value of the QoI, and quantifies the magnitude of this change. In this study, the QoI is computed using the governing equations presented in the previous section. In order to extract the sensitivity information, a method needs to be devised to efficiently compute the gradient (Jacobian) of these governing equations.

Several approaches exist, in order to compute gradients from a system of equations [42]: analytical computation, numerical approximation, etc. As far as numerical techniques are concerned, the most common method is the finite difference approach. This method consists of adding a small perturbation to the parameter with respect to which the sensitivity is being computed. The non-linear equations are then solved with the perturbed quantity, and the difference between the resulting value and the original (unperturbed) one divided by the perturbation provides a first order approximation of the gradient. This method quickly becomes too expensive for large systems of non-linear equations, with multiple parameters of interest, since it commands multiple (potentially unsteady) simulations. In addition, optimal value of the selected perturbation changes from case to case and parameter to parameter, making it non-trivial and non-robust in practice, where often suboptimal values can lead to large variations in the estimated values of the gradient.

An alternative method is the forward sensitivity approach, which is based on the linearization of the governing equations to provide evolution equations for the gradient with respect to a single parameter. The main advantages of the forward sensitivity method are (i) the non-linear problem needs to be solved once and (ii) the gradient of any quantity of interest with respect to a certain parameter is computed from a linear system of equations, more easily solved than the non-linear equations. The main disadvantage of this approach, which also renders it impractical for systems with large parameter spaces, is that for each parameter, a separate equation needs to be derived, discretized, and solved numerically. Nonetheless, the forward sensitivity approach is also presented here, and will be used to validate a third method for gradient computation, namely the adjoint method. The latter indeed proves superior in the context of this study, and will therefore be discussed subsequently.

3.1 Forward sensitivity

A brief description of the forward sensitivity approach is presented below for a Differential Algebraic Equation given as;

$$\begin{cases} \frac{d\mathbf{u}^d}{d\tau}(\tau) = \mathbf{F}^d[\tau, \mathbf{u}^a(\tau), \mathbf{u}^d(\tau), \mathbf{p}], \\ \mathbf{0} = \mathbf{F}^a[\tau, \mathbf{u}^a(\tau), \mathbf{u}^d(\tau), \mathbf{p}] \end{cases} \quad (22)$$

where, $\mathbf{u} = (\mathbf{u}^a, \mathbf{u}^d)$ denotes the dependent variable, also known as the state vector. In the case of unsteady char burnout presented here, the state vector is composed of differential variables \mathbf{u}^d (density, species mass fraction and gas phase temperature) on the one hand, and an algebraic variable \mathbf{u}^a (radial coordinate) on the other hand. \mathbf{p} represents the parameters of interest. The algebraic operator \mathbf{F}^a contains the discretization of the mapping equation. The differential operator \mathbf{F}^d represents the semi-discretization of the transport equations that also includes Robin and Dirichlet boundary conditions, at the particle surface and in the far-field, respectively. In the literature, equation 22 is referred to as a Differential Algebraic Equation (DAE) of index-1. It differs from Ordinary Differential Equations (ODE) in that the rate of change of the algebraic variable \mathbf{u}^a does not appear explicitly. For more information regarding the classification of such equations, the reader is referred to [6].

In the context of adjoint-based sensitivity analysis, equation 22 is commonly known as the primal or forward problem (in the problem of interest to this study, the forward problem is given by the governing equations described in the previous section). The forward problem can be linearized as follows,

$$\begin{cases} \frac{d\mathbf{u}_p^d}{d\tau} = \frac{\partial \mathbf{F}^d}{\partial \mathbf{u}} \Big|_{\tau, \mathbf{p}} \mathbf{u}_p + \frac{\partial \mathbf{F}^d}{\partial \mathbf{p}} \Big|_{\tau, \mathbf{u}} \\ \mathbf{0} = \frac{\partial \mathbf{F}^a}{\partial \mathbf{u}} \Big|_{\tau, \mathbf{p}} \mathbf{u}_p + \frac{\partial \mathbf{F}^a}{\partial \mathbf{p}} \Big|_{\tau, \mathbf{u}} \end{cases}, \quad (23)$$

where

$$\mathbf{u}_p = \frac{\partial \mathbf{u}}{\partial p} \quad (24)$$

denotes the sensitivity with respect to p , any given component of \mathbf{p} . As it appears, the main drawback of the forward sensitivity approach is that it requires re-deriving the second term on the right hand side of equation 23 for each selected parameter p , which becomes a disadvantage for systems with large numbers of parameters. The adjoint method is then more apt to deal with this shortcoming [13], as highlighted in the following section.

As the derivation of forward sensitivity equation does not depend on the quantity of interest (QoI), the sensitivity with respect to any QoI can be computed using the initial condition of the following form,

$$\mathbf{u}_p(0) = \mathbf{0}. \quad (25)$$

Here, only time-integrated QoIs, denoted as G , are considered, leading to

$$G = \int_0^{\mathcal{T}} g[\tau, \mathbf{u}(\tau), \mathbf{p}] d\tau, \quad (26)$$

where, g denotes the instantaneous value of the QoI, and \mathcal{T} the final time horizon. The expression describing the sensitivity is then given, in normalised form, as

$$\frac{dG}{dp} = \frac{\|p\|}{G} \left[\int_0^{\mathcal{T}} \left(\frac{\partial g}{\partial \mathbf{u}} \Big|_{\tau, \mathbf{p}} \mathbf{u}_p + \frac{\partial g}{\partial p} \Big|_{\tau, \mathbf{u}} \right) d\tau \right]. \quad (27)$$

Normalising the extracted sensitivity by the value of the parameter and the QoI, leads to a non-dimensionalized gradient, and allows a fair comparison between sensitivities of various QoIs with respect to different parameters.

3.2 Discrete adjoint

This section briefly describes the extraction of discrete adjoint equations, for a DAE of index-1, as represented by equation 22 (a detailed description is provided in [6]).

Considering a general QoI, G , the first step to derive the adjoint equation is to construct the Lagrange functional as follows,

$$L = G(\mathbf{u}^a, \mathbf{u}^d, \mathbf{p}) - \int_0^{\mathcal{T}} \boldsymbol{\eta}^d \cdot \left\{ \frac{d\mathbf{u}^d}{d\tau} - \mathbf{F}^d[\tau, \mathbf{u}^a(\tau), \mathbf{u}^d(\tau), \mathbf{p}] \right\} d\tau + \int_0^{\mathcal{T}} \boldsymbol{\eta}^a \cdot \mathbf{F}^a[\tau, \mathbf{u}^a(\tau), \mathbf{u}^d(\tau), \mathbf{p}] d\tau, \quad (28)$$

where initial conditions have been omitted for clarity. $G(\mathbf{u}^a, \mathbf{u}^d, \mathbf{p})$ is a general representation for a semi-discrete quantity of interest. $\boldsymbol{\eta}^d$ and $\boldsymbol{\eta}^a$ are the algebraic and differential adjoint variables respectively. In order to extract the adjoint equation, the variation of the Lagrange functional with respect to the state vector $\mathbf{u} = (\mathbf{u}^d, \mathbf{u}^a)$ is set to zero. The resulting equations are presented in the next sections for special cases of a time-integrated QoI and a local QoI.

3.2.1 Time-integrated quantity of interest

Let us first consider the case of a time-integrated quantity of interest:

$$G = \int_0^{\mathcal{T}} g[\tau, \mathbf{u}^a(\tau), \mathbf{u}^d(\tau), \mathbf{p}] d\tau. \quad (29)$$

Setting the variation of the Lagrange functional (equation 28) with respect to the state vector to zero, leads to the following adjoint equations,

$$\frac{d\boldsymbol{\eta}^d}{d\tau} + \left(\frac{\partial \mathbf{F}^d}{\partial \mathbf{u}^d} \right)^\dagger \boldsymbol{\eta}^d + \left(\frac{\partial \mathbf{F}^a}{\partial \mathbf{u}^d} \right)^\dagger \boldsymbol{\eta}^a = -\frac{\partial g}{\partial \mathbf{u}^d}, \quad (30)$$

$$\left(\frac{\partial \mathbf{F}^d}{\partial \mathbf{u}^a} \right)^\dagger \boldsymbol{\eta}^d + \left(\frac{\partial \mathbf{F}^a}{\partial \mathbf{u}^a} \right)^\dagger \boldsymbol{\eta}^a = -\frac{\partial g}{\partial \mathbf{u}^a} \quad (31)$$

where \dagger denotes the transpose operator. In this case, the initial condition for the adjoint equation is,

$$\boldsymbol{\eta}^d(\mathcal{T}) = \mathbf{0}. \quad (32)$$

As can be deduced from the initial condition, the adjoint equation needs to be integrated backward in time. As a result, this equation is sometimes referred to as the backward problem, as opposed to the forward (primal) problem,

which is integrated forward in time. The terms in equations 30 & 31 include jacobians of \mathbf{F}^d , \mathbf{F}^a and g , evaluated using the forward solution, suggesting that the solution of the forward problem is needed at each time step of the backward integration. This solution must either be already stored in memory, or recalculated from the solution at the last stored time step. This procedure is called checkpointing, which is also employed in this study to make the forward solution available in the adjoint integration step.

The sensitivity can then be computed by linearizing the discrete version of the Lagrange functional with respect to parameter \mathbf{p} , leading to:

$$\frac{dG}{d\mathbf{p}} = \int_0^{\mathcal{T}} \left(\frac{\partial g}{\partial \mathbf{p}} + \boldsymbol{\eta}^d \cdot \frac{\partial \mathbf{F}^d}{\partial \mathbf{p}} + \boldsymbol{\eta}^a \cdot \frac{\partial \mathbf{F}^a}{\partial \mathbf{p}} \right) d\tau. \quad (33)$$

The extracted gradient can then be normalised for each parameter, as is done in equation 27.

3.2.2 Local quantity of interest

A local (in time) quantity of interest can also be considered as follows:

$$g^\sigma = g(\sigma, \mathbf{u}^d(\sigma), \mathbf{u}^a(\sigma), \mathbf{p}). \quad (34)$$

In the above equation, σ denotes the time instance where the sensitivity is computed. Setting the variation of the Lagrange functional with respect to the state variable to zero leads to,

$$\frac{d\boldsymbol{\eta}^d}{d\tau} + \left(\frac{\partial \mathbf{F}^d}{\partial \mathbf{u}^d} \right)^\dagger \boldsymbol{\eta}^d + \left(\frac{\partial \mathbf{F}^a}{\partial \mathbf{u}^d} \right)^\dagger \boldsymbol{\eta}^a = \mathbf{0}, \quad (35)$$

$$\left(\frac{\partial \mathbf{F}^d}{\partial \mathbf{u}^a} \right)^\dagger \boldsymbol{\eta}^d + \left(\frac{\partial \mathbf{F}^a}{\partial \mathbf{u}^a} \right)^\dagger \boldsymbol{\eta}^a = \mathbf{0}. \quad (36)$$

It should be noted that, the adjoint equations are not driven by the QoI (the right-hand-sides of both equations are zero). Also, in contrast to the time-integrated quantities, the general expression for the initial condition shows explicit dependence on the QoI as follows,

$$\boldsymbol{\eta}^d(\sigma) = \frac{\partial g}{\partial \mathbf{u}^d} \Big|_\sigma - \frac{\partial \mathbf{F}^a}{\partial \mathbf{u}^d} \Big|_\sigma \left(\frac{\partial \mathbf{F}^a}{\partial \mathbf{u}^a} \Big|_\sigma \right)^{-1} \frac{\partial g}{\partial \mathbf{u}^a} \Big|_\sigma. \quad (37)$$

In the case where the QoI is independent of the algebraic variable, the initial condition (37) simplifies to:

$$\boldsymbol{\eta}^d(\sigma) = \frac{\partial g}{\partial \mathbf{u}^d} \Big|_\sigma. \quad (38)$$

Finally, the sensitivity with respect to the parameter \mathbf{p} is given by,

$$\frac{dg^\sigma}{d\mathbf{p}} = \frac{\partial g}{\partial \mathbf{p}} \Big|_\sigma + \int_0^\sigma \left(\boldsymbol{\eta}^d \cdot \frac{\partial \mathbf{F}^d}{\partial \mathbf{p}} + \boldsymbol{\eta}^a \cdot \frac{\partial \mathbf{F}^a}{\partial \mathbf{p}} \right) d\tau. \quad (39)$$

4 Discretization and numerical solution

This section discusses the discretization and subsequent solution of the non-linear, unsteady problem and the related linear sensitivity and adjoint equations. The method of lines is used to transform the algebraic partial differential equations into algebraic ordinary differential equations by discretizing the spatial operators. In order to ensure the stability of the problem, a first order upwind scheme is used to discretize the convective term, and a central second order scheme is used to discretize the diffusive and conductive terms. The source terms are treated locally. The spatial dimension is discretized using a regular equidistant mesh. The variables are collocated at the center of their corresponding cell. As previously mentioned, the discretization is performed in the mass-based coordinate (ψ, τ) , described in equation 8. When a quantity needs to be evaluated in physical space, a change of coordinates is performed back into the physical coordinates (r, t) .

A fully implicit time integrator (CVODE [17]) is used to advance the equations in time. Forward sensitivity and adjoint equations are discretized in a similar fashion as the equations of the non-linear problem. Due to existing unsteadiness, the linearized equations depend on the values of the unsteady state variables, and a checkpointing algorithm is required. The pseudo-spatial (mass-based) grids for forward sensitivity and adjoint problems are kept identical to the ones used for the non-linear problem. However, interpolation within the time steps of the time integrator is still required. The time steps are chosen small enough to minimise the error due to interpolation between checkpoints.

The species, temperature, and density profiles are initialized as constants. The last variable, r , is initialized to satisfy the mapping equation 8. This is achieved by the following the closed-form solution

$$r_i = \alpha + 1 \sqrt{r_{i-1}^{\alpha+1} + (\alpha + 1) \frac{\Delta\psi_{i-1}}{\rho_i}}. \quad (40)$$

The initial condition for the differential adjoint variables $\boldsymbol{\eta}^d$ are discussed in section 3.2. An initial value also needs to be prescribed for the algebraic adjoint variables $\boldsymbol{\eta}^a$, which is done as follows,

$$\boldsymbol{\eta}^a = \left(\frac{\partial g}{\partial \mathbf{u}^a} - \boldsymbol{\eta}^d \cdot \frac{\partial \mathbf{F}^d}{\partial \mathbf{u}^a} \right) \left(\frac{\partial \mathbf{F}^a}{\partial \mathbf{u}^a} \right)^{-1}. \quad (41)$$

The resulting discretized equations are implemented using a recently developed language, Julia [9], targeted at scientific computing applications. Julia leverages state-of-the-art compiler technologies to deliver performance comparable to traditional statically-typed languages while guaranteeing the productivity expected from dynamic languages.

5 Results and Validation

The results are presented for two different environments, as illustrated in Table 1. The oxy environment is of interest in coal combustion as one of viable methods to reduce CO₂ emissions [7]. In an oxy environment, air is replaced by pure oxygen (O₂) or a mixture of oxygen with recycled flue gas, generating high CO₂ concentrations and causing the combustion process to change significantly. The composition of both environments is shown in table 1, which closely matches the experimental condition of the flat flame burner of Schiemann *et al.* [35], later simulated by Farazi *et al.* [11].

Test case	Diluent	$Y_{O_2}^\infty$	Y_{CO}^∞	$Y_{CO_2}^\infty$	$Y_{N_2}^\infty$
Air atmosphere	N ₂	0.326	0.0	0.105	0.569
Oxy atmosphere	CO ₂	0.262	0.0	0.738	0.0

Table 1: Compositions defining air and oxy atmospheres in this study.

5.1 Forward (primal) problem

In this section, the results of the primal problem is presented and compared between air and oxy atmospheres. The pressure P is set to 10⁵Pa, and the far-field temperature T^∞ is 1673K. The initial particle radius is set to $r_0 = 60 \times 10^{-6}$ m. It should be noted that devolatilisation is not accounted for in this study. As a result, the initial particle temperature is assumed to be $T_p^0 = 1200$ K.

Figure 1 shows the variation of temperature and relevant mass fractions, from their initial to final distributions, for air atmosphere. In order to better illustrate the initial variation of selected QoIs in this study (for example, burning rate, discussed later in this section), time variable t is transformed to $t^* = \ln(t/\Delta t)$, where $\Delta t = 1.25 \times 10^{-11}$ s. Initially, due to the transfer of heat from the surrounding hot gas to the cooler particle, the gas temperature in the particle vicinity starts to decrease, as shown in figure 1a. As time evolves, the difference between particle and gas phase temperatures decreases. Finally, the heat released by the system is not completely absorbed by the particle, leading to an increase in the gas phase temperature close to the particle surface. This behaviour can be better observed by comparing the temperature distributions at $t^* = 22.14$ and $t^* = 27$. Due to the presence of heterogeneous reactions on the surface (char oxidation reaction, in particular), oxygen mass fraction reduces close to the particle surface, as illustrated in figure 1b. Carbon dioxide mass fraction, on the other hand, increases initially close to the particle surface, and after reaching a peak, decreases to the far-field value (figure 1c). The peak in carbon dioxide mass fraction, as a product of the gas phase reaction,

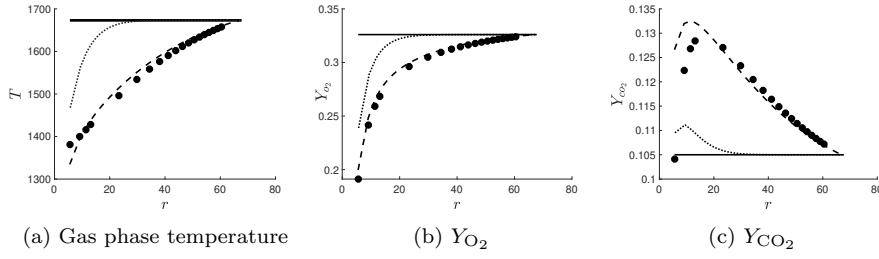


Fig. 1: Evolution of spatial distribution of temperature, oxygen mass fraction (Y_{O_2}), and carbon dioxide mass fraction (Y_{CO_2}) in the spatial domain, for air atmosphere: —, ($t^* = 10^{-10}$); \cdots , ($t^* = 18.85$); — —, ($t^* = 22.14$); \bullet , ($t^* = 27$).

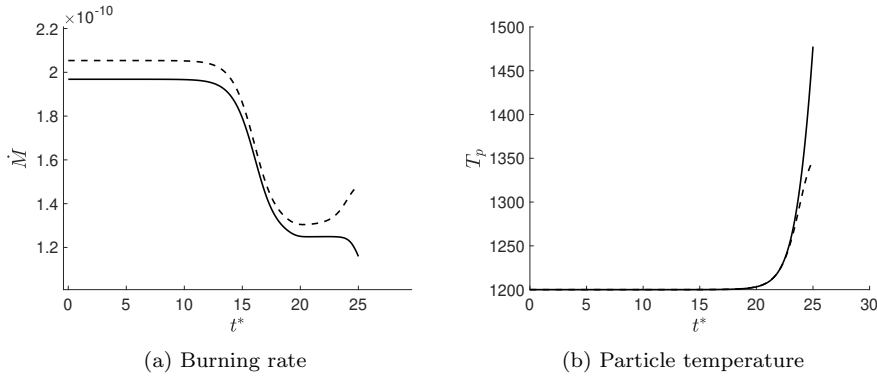


Fig. 2: Evolution of particle temperature and burning rate in time: —, air; — —, oxy atmosphere.

gives and indication of the flame position in the gas phase. Carbon dioxide is consumed by the char reaction, leading to the decrease of its mass fraction value close to the particle surface.

While analysing the evolution of certain quantities in the spatial domain can be informative, investigating the changes in quantities such as particle temperature and burning rate, measurable in both experiments and simulations, are more relevant to this study. Figure 2 shows the evolution of the particle temperature and its burning rate $\dot{M} = \dot{M}_w r_0^3$ for air and oxy atmospheres. Since the interest of this study lies in analysing the transient behaviour of the problem, the simulations are stopped when the ratio of the burnt coal M_b/M_0 reaches 5.3%. Here, M_b is the burnt mass of the particle, and M_0 is the initial mass of the particle. This time-frame ensures that the problem does not reach a steady state.

Burning rate is an important QoI, since it expresses the consumption rate of the particle and sets the value of the Stefan flow velocity. In both cases, three distinct regions can be identified as far as the burning rate is concerned: (i) the short time behaviour, where the burning rate remains relatively constant, followed by (ii) the intermediate time behaviour where the burning rate reduces, reaching a plateau, and finally, (iii) the long time behaviour where the burning rate increases in the oxy atmosphere and continues to decrease in the air atmosphere. This change in the long time behaviour, is due to the fact that, the particle temperature starts to reach an asymptotic value in the oxy atmosphere as opposed to air, where the temperature continues to increase (figure 2b). Similar trends were observed in two-dimensional unsteady simulations of Farazi *et al.* [11]. As far as the short time behaviour of the burning rate is considered, the oxy atmosphere leads to higher burning rates compared to air, a trend that persists in time. It should however be noted that these results are valid for cases where the initial devolatilisation process can be ignored.

Considering the variation in the particle temperature, it can be noted that, initially, due to weaker heterogeneous reactions on the particle surface (low reaction rates), particle temperature increases slightly (this variation is not visible in the profiles of figure 2b). At this stage, the particle is heated mainly through heat conduction between the hot gas and the cooler particle. However, as the simulation advances and reaches the long time behaviour, particle temperature rapidly increases, as both heterogeneous and homogeneous reactions become stronger. Comparing the two atmospheres, the heating rate for the particle in air is higher than in oxy atmosphere.

Particle temperature and burning rate will be used in the following section as quantities of interest, and help identify sensitivities with respect to model/physical parameters.

5.2 Sensitivities of unsteady char combustion

In this section, the sensitivities computed with the adjoint method (section 3.2) are compared to those computed using the forward sensitivity method (section 3.1). Once validated, sensitivities are then extracted for both air and oxy atmospheres, and the evolution of the extracted sensitivities in time are compared and analysed. Note that the extracted sensitivities are all in non-dimensional form, as described in section 3.

5.2.1 Cross-validation of adjoint and forward sensitivity

In this section, the sensitivities computed using the adjoint and forward sensitivity methods are compared and analysed. Due to the unsteady nature of the problem, the objective function (quantity of interest), G , is defined as an time-integrated quantity (see section 3.2). Therefore, before extracting the resulting sensitivities, the time horizon for integration \mathcal{T} needs to be defined.

Figure 3 compares the sensitivities extracted using discrete adjoint and forward sensitivity techniques for $\mathcal{T}^* = 20.92$. Here, the particle temperature is selected as the quantity of interest, leading to the following definition of the objective function,

$$G = \int_0^{\mathcal{T}} T_p dt. \quad (42)$$

Figure 2a shows that, within this time horizon, the system demonstrates an intermediate time behaviour, where the burning rate is time-dependent (in the following section, the dependence of sensitivities on the selected time horizon is further analysed). Figure 3 shows good agreement between the extracted sensitivities through the forward sensitivity and the discrete adjoint techniques for various heat conductivities (λ_g). Further analysis shows that this agreement is independent of the selected time horizon and the parameter of interest. Therefore, in the following section only the discrete adjoint method is used to compute the sensitivities.

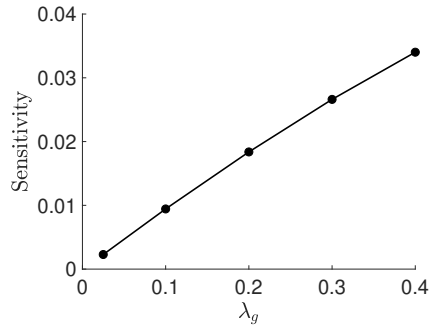


Fig. 3: Sensitivity of particle surface temperature, T_p , with respect to gas conductivity (λ_g):—, discrete adjoint; •, forward sensitivity.

5.2.2 Time variable sensitivities

Since the burning rate is the most relevant QoI to this study, the evolution of parameter sensitivities are first extracted for the burning rate. Therefore, QoI is formally defined as,

$$G = \int_0^{\mathcal{T}} \dot{M}_w dt. \quad (43)$$

Figure 4 compares the sensitivities extracted in both air and oxy atmospheres, where $\mathcal{T}^* = 22.9$ and the burning rate has reached a plateau, as illustrated by figure 2a. In figure 4, the focus has been placed on the heterogeneous and homogeneous kinetic model parameters (such as activation energies and pre-exponential factors). Sensitivity with respect to the heat conductivity of the

gas phase λ_g is also computed, since it governs the heat conduction from the gas to the particle and directly affects the burning rate (see section 2).

Figure 4 shows that, regardless of the free stream composition, the sensitivity of burning rate to the parameters of the homogeneous reaction are smaller than those of the heterogeneous reactions. This result can change if more complex models are considered. As far as the heterogeneous reactions are concerned, the char oxidation reaction seems to be the most dominant. In both free stream compositions, the burning rate shows higher sensitivities with respect to the parameters of the oxidation reaction, and in particular, the activation energy, which shows the highest sensitivity in both cases. When comparing the results of the two atmospheres, air seems to result in higher sensitivities than oxy atmosphere, due to the higher heating rate of char in air. These results are however extracted for a selected time horizon. Therefore, it would be of interest to investigate the evolution of these sensitivities as the time horizon is varied.

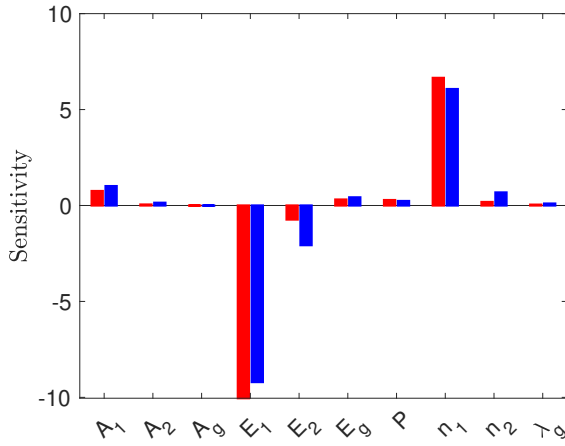


Fig. 4: Sensitivities extracted for burning rate with respect to kinetic model parameters at $t^* = 22.9$. (red), air; (blue), oxy atmosphere.

In order to extract time-varying sensitivities, term \mathcal{T} in equation 43 is varied, and sensitivities are extracted for discrete time intervals. The results are shown in figure 5, and are compared for the two free stream compositions. Judging by the result of figure 4, showing the final distribution of the overall sensitivities at $\mathcal{T}^* = 22.9$, burning rate is expected to show highest sensitivities with respect to the parameters of the oxidation reaction, confirmed by the results of figure 5. This figure also shows that, all parameter sensitivities are initially constant, following the same behaviour as the burning rate for short time horizons, as shown in figure 2a. For longer time horizons, while the decrease in burning rate influences the sensitivities of some of the parame-

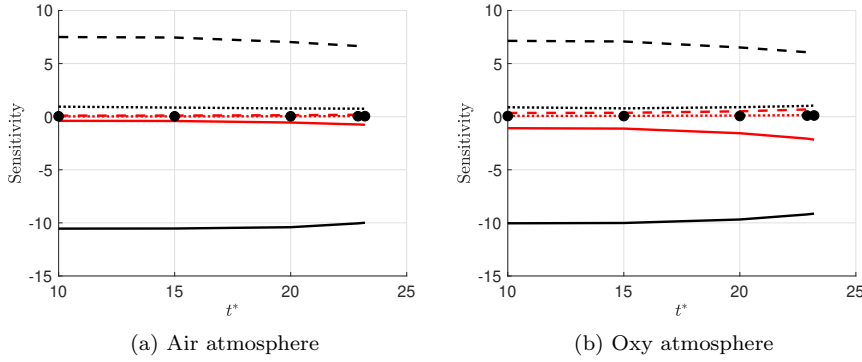


Fig. 5: Evolution of sensitivities, extracted for burning rate, \dot{M} , as QoI, for air and oxy atmospheres: —, E_2 ; - - -, n_2 ; ···, A_2 ; —, E_1 ; - - -, n_1 ; ···, A_1 ; •, λ_g .

ters, the sensitivities of the dominant parameters seem to be unaffected. As the time horizon does not affect the sensitivities extracted for the most dominant parameters, the short time behaviour can be used as a surrogate for the overall sensitivity distribution. Comparison of figures 5a and 5b suggests that the free stream composition does not affect model sensitivities measured by choosing burning rate as QoI. The negligible effect of free stream composition on burning rate sensitivities can be attributed to slower diffusion time scale, which compared to the selected time horizon \mathcal{T}^* leads to insufficient time for the effect of the free stream to propagate to the surface of the particle.

In order to examine the effect of the choice of the QoI on the extracted sensitivities, a configuration similar to the one examined in figure 4 is selected. Sensitivities are however extracted with respect to particle surface temperature, as presented in equation 42. The results are shown in figure 6. This figure demonstrates that the choice of the QoI affects the distribution of sensitivities for both free stream compositions. While the most sensitive parameters remain the parameters of the direct oxidation reaction, as was the case for the burning rate, the most dominant parameter is now the pre-exponential factor with the activation energy following closely. The parameters of the second heterogeneous reaction show relatively higher sensitivities, as far as the prediction of the particle temperature is concerned. Comparing figures 4 and 6 also shows overall higher sensitivities for burning rate than particle temperature, suggesting that uncertainties in the value of these parameters would result in higher discrepancies in the burning rate prediction, rather than particle temperature. In order to determine whether this behaviour is independent of the selected time horizon, the evolution of sensitivities need to be extracted as a function of time.

Figure 7 shows the evolution of the particle temperature sensitivities with respect to the heterogeneous reaction parameters. The evolution of sensitivities

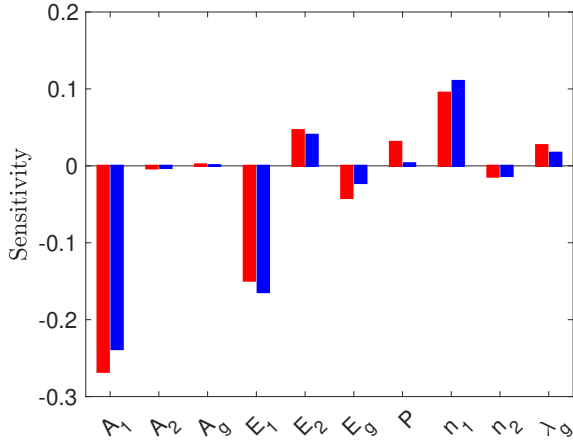


Fig. 6: Sensitivities extracted for particle temperature T_p with respect to kinetic model parameters at $t^* = 22.9$. (red), air; (blue) oxy atmosphere.

is entirely different to what was observed in figure 5. This change is due to the different behaviours of the two quantities of interest, as illustrated in figure 2. While the burning rate is initially constant and then decreases, the particle temperature monotonically increases, with an abrupt increase at the end of the considered time horizon. The sensitivities of the particle temperature follow a similar trend. The parameters of the direct oxidation reaction remain the most sensitive with the pre-exponential factor dominating the sensitivities of the particle temperature. Comparing the particle temperature sensitivities extracted in the two environments shows that air yields slightly higher values as far as the pre-exponential factor is concerned.

Regardless of the free stream composition and the time horizon, selecting burning rate as the quantity of interest leads to larger values in parameter sensitivities compared to the particle temperature, suggesting the burning rate to be the more relevant choice of QoI for this problem. This is expected, since the value of the Stephan flow velocity on the surface of the particle governs the dynamics of the underlying system.

Finally, sensitivities with respect to physical conditions of the system are extracted. Here, free stream mass fractions are chosen as the parameters of interest, since when determining surface model parameters experimentally, curves are fitted considering these quantities. High sensitivities with respect to free stream conditions can lead to inaccuracy in determination of model coefficients. Earlier, the burning rate was established as the most relevant quantity of interest to this problem. As a result, these sensitivities are reported only for the burning rate. They are shown in figure 8 where they are compared for the two free stream compositions. In contrast to the sensitivities with respect to model parameters (figure 5), the sensitivities with respect to free stream mass

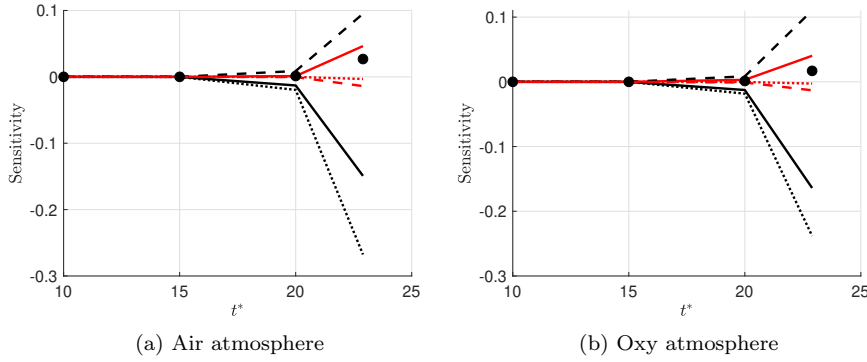


Fig. 7: Evolution of sensitivities, extracted for particle temperature, T_p , as QoI, for air and oxy atmospheres: —, E_2 ; ---, n_2 ; ···, A_2 ; —, E_1 ; ---, n_1 ; ···, A_1 ; •, λ_g .

fractions show more dependence on the selected time horizon. However, the resulting non-dimensionalized sensitivities are considerably lower than those extracted with respect to kinetic model parameters. Comparing the sensitivities of the two free stream compositions shows that, since the problem is diffusion controlled, the diluting species (N_2 for air and CO_2 for oxy atmosphere), plays an important role and results in the highest sensitivities. This is followed by sensitivities in oxygen mass fraction in both free stream compositions, as oxygen consumption is an exothermic reaction of char oxidation and contributes the most to the burning rate. Carbon monoxide shows minimum sensitivity in both air and oxy atmospheres, due to the weak gasification reactions on the surface and in the gas phase.

In conclusion, while interpreting the results presented in this section, the following points need to be considered. Firstly, working within the perimeter of the kinetic models chosen in this study, the extracted sensitivities are directly dependent on the accuracy of the predicted solution, as measured and identified from the model. This does not guarantee that these sensitivities match experimental observations. The differences, however, motivate the use of more sophisticated models in their stead. Secondly, the extracted sensitivities are directly dependent on the choice of QoI. While one QoI might lead to high sensitivities with respect to a model parameter or physical composition of the problem, another QoI might show no sensitivities at all. Therefore, if the QoI is not chosen correctly, it might have misleading consequences in the interpretation of the extracted sensitivities.

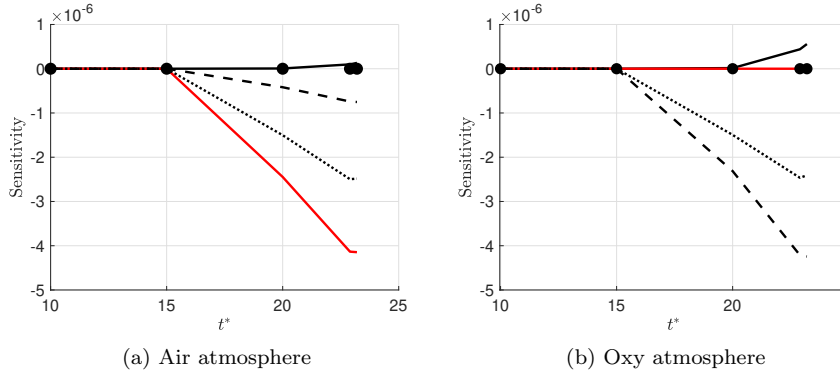


Fig. 8: Evolution of free stream sensitivities, extracted for burning rate, \dot{M} , as QoI, for air and oxy atmospheres: —, N_2^∞ ; —, T^∞ ; - - -, CO_2^∞ ; ···, O_2^∞ ; •, CO^∞ .

6 Conclusion

An adjoint-based technique is used to analyse existing model sensitivities in numerical predictions of unsteady char particle combustion. These models are employed in order to describe the reactions on the surface of the particle (heterogeneous reactions) as well as in the gas phase (homogeneous reactions), and include multiple model parameters in their definition. As a result, the determination of model sensitivities in the prediction of certain quantities of interest is only possible by extracting sensitivities with respect to the existing model parameters. In addition to the model parameters, another important factor in char combustion is the free stream composition. Due to success of oxy environments in reducing CO₂ emissions, air is commonly replaced by pure oxygen (O₂) or a mixture of oxygen with recycled flue gas, leading to variable free stream compositions. Therefore, the impact of free stream composition on the sensitivities need to be quantified as well.

In this study, we illustrate the use of the adjoint methodology as a viable approach to extract such sensitivities. This approach proves to be more effective than the forward sensitivity method, since it alleviates the solution of multiple forward sensitivity equations as the parameter of interest is altered. Using the adjoint method, the sensitivities with respect to all existing parameters are extracted with essentially one forward and backward sweep of the primal and adjoint equations, making it a suitable alternative for systems with large sets of model parameters.

Sensitivities were extracted for variable quantities of interest in two free stream compositions, determined by the flat flame burner experiments of Schiemann *et al.* [35] and corresponding to air and oxy environments. When the particle burning rate is considered as the QoI, the parameters of the first surface reaction (direct oxidation reaction) prove to be the most dominant, and in

particular, the activation energy. This dominance remains independent of the selected time horizon (short or long) and the free stream composition. On the other hand, a shift of the QoI to particle temperature changes both the distribution of sensitivities at a selected time instance and their evolution in time. In the case of particle temperature, the pre-exponential factor seems to be the most sensitive parameter and its sensitivity steadily increases in time. This is due to the difference in the evolution of the particle temperature and the burning rate in time. However, regardless of the free stream composition, the burning rate shows higher sensitivities with respect to the model parameters, suggesting this quantity to be the most relevant in such sensitivity analyses. Burning rate sensitivities with respect to free stream variables show that the diluent species has the highest sensitivity, with the oxygen mass fraction following closely. However, the sensitivities with respect to free stream values are considerably lower than the sensitivities extracted for heterogeneous model parameters, suggesting these models to be the main source of sensitivity in the system.

Acknowledgements The authors kindly acknowledge financial support through Deutsch Forschungsgemeinschaft (DFG) through SFB/TRR 129.

References

1. Baum, M., Street, P.: Predicting the combustion behaviour of coal particles. *Combust. Sci. Technol.* **3**(5), 231–243 (1971)
2. Beck, N., Hayhurst, A.: The early stages of the combustion of pulverised coal at high temperatures i: the kinetics of devolatilization. *Combust. Flame* **79**(1), 47–74 (1990)
3. Bewley, T., Moin, P., Temam, R.: Dns-based predictive control of turbulence: an optimal benchmark for feedback algorithms. *J Fluid Mech.* **447**, 179–225 (2001)
4. Braman, K., Oliver, T., Raman, V.: Adjoint-based sensitivity analysis of flames. *Comb. Theo. Modelling* **19**(1), 29–56 (2015)
5. Cai, L., Uygun, Y., Togbe, C., Pitsch, H., Olivier, H., Dagaut, P., Sarathy, S.: An experimental and modeling study of n-octanol combustion. *Proc. Combust. Inst.* **35**, 419–427 (2015)
6. Cao, Y., Li, S., Petzold, L., Serban, R.: Adjoint sensitivity analysis for differential-algebraic equations: the adjoint dae system and its numerical solution. *SIAM J. Sci. Comput* **24**(3), 1076–1089 (2003)
7. Chen, L., Yong, S., Ghoniem, A.: Oxy-fuel combustion of pulverized coal: characterization, fundamentals, stabilization and cfd modeling. *Prog. Energy Combust. Sci.* **38**(2), 156–214 (2012)
8. Duraisamy, K., Alonso, J.: Adjoint-based techniques for uncertainty quantification in turbulent flows with combustion. 42nd AIAA Fluid Dynamics Conference and Exhibit pp. 25–28 (2012)
9. Edelman, J.B.A., Karpinski, S.: Julia: A fresh approach to numerical computing. *SIAM* **59**(1), 65–98 (2020)
10. Essenhigh, R.: Predicted burning times of solid particles in an idealized dust flame. *J Inst Fuel* **34**, 239–44 (1961)
11. Farazi, S., Sadr, M., Kang, S., Schiemann, M., Vorobiev, N., Scherer, V., Pitsch, H.: Resolved simulations of single char particle combustion in a flow field. *Fuel* **201**, 15–28 (2017)
12. Foures, D., Caulfield, C., Schmid, P.: Optimal mixing in two-dimensional plane poiseuille flow at finite peclet number. *J Fluid Mech.* **748**, 241–277 (2014)

13. Giles, M., Pierce, N.: An introduction to the adjoint approach to design. *Flow Turb. Combust.* **65**, 393–415 (2000)
14. Ha, M., Choi, B.: A numerical study on the combustion of a single carbon particle entrained in a steady flow. *Combust. Flame* **97**, 1–16 (1994)
15. Hecht, E., Shaddix, C., Lighty, J.: Analysis of the errors associated with typical pulverized coal char combustion modeling assumptions for oxy-fuel combustion. *Combust. Flame* **160**(8), 1499–509 (2013)
16. Higuera, F.: Combustion of a coal char particle in a stream of dry gas. *Combust. Flame* **152**(1), 230–244 (2008)
17. Hindmarsh, A., Brown, P., Grant, K., Lee, S., Serban, R., Shumaker, D., Woodward, C.: SUNDIALS: suite of nonlinear and differential/algebraic equation solvers. *ACM Transactions on Mathematical Software* **31**(3), 363–396 (2005)
18. Jameson, A.: Aerodynamic shape optimization using the adjoint method. *Lectures at the Von Karman Institute* (2003)
19. Juniper, M.: Triggering in the horizontal rijke tube: non-normality, transient growth and bypass transition. *J Fluid Mech.* **667**, 272–308 (2010)
20. Kestel, M., Nikrityuk, P., Hennig, O., Hasse, C.: Numerical study of the partial oxidation of a coal particle in steam and dry air atmospheres. *IMA J Appl. Math* **77**(1), 32–46 (2012)
21. Lee, J., Tomboulides, A., Orszag, S., Yetter, R., Dryer, F.: A transient two-dimensional chemically reactive flow model: Fuel particle combustion in a nonquiescent environment. *Symp Int. Combust.* **26**(2), 3059–65 (1996)
22. Lee, J., Yetter, R., Dryer, F.: Numerical study of the partial oxidation of a coal particle in steam and dry air atmospheres. *Combust. Flame* **101**, 387–398 (1995)
23. Lemke, M., Cai, L., Reiss, J., Pitsch, H., Sesterhehn, J.: Adjoint-based sensitivity analysis of quantities of interest of complex combustion models. *Comb. Theo. Modelling* **23**(1), 180–196 (2019)
24. Lemke, M., Reiss, J., Sesterhehn, J.: Adjoint-based analysis of thermoacoustic coupling. *ICNAAM* **667**, 2163–2166 (2013)
25. Libby, P., Blake, T.: Theoretical study of burning carbon particles. *Combust. Flame* **36**, 139–169 (1979)
26. Libby, P., Blake, T.: Burning carbon particles in the presence of water vapor. *Combust. Flame* **41**, 123–147 (1981)
27. Makino, A.: An approximate explicit expression for the combustion rate of a small carbon particle. *Combust. Flame* **90**, 143–154 (1992)
28. Matalon, M.: Complete burning and extinction of a carbon particle in an oxidizing atmosphere. *Combust. Sci. Technol.* **24**, 115–127 (1980)
29. McConnell, J., Sutherland, J.: The effect of model fidelity on prediction of char burnout for single-particle coal combustion. *Proc. Combust. Inst.* **36**(2), 2165–72 (2016)
30. Nusselt, W.: Der verbrennungsvorgang in der kohlenstaubfeuerung. *Z Ver Deut Ing* **68**, 125–8 (1924)
31. Pironneau, O.: On optimum design in fluid mechanics. *J Fluid Mech.* **64**(1), 97–110 (1974)
32. Rabin, S., Caulfield, C., Kerswell, R.: Designing a more nonlinearly stable laminar flow via boundary manipulation. *J Fluid Mech.* **738 R1**, 1–12 (2014)
33. Safran, N., Lotz, J., Naumann, U.: Algorithmic differentiation of numerical methods: Second-order adjoint solvers for parameterized systems of nonlinear equations. *Procedia Computer Science* **80**, 2231–2235 (2016)
34. Saltelli, A., Ratto, M., Tarantola, S., Campolongo, F.: Sensitivity analysis for chemical models. *Chem. Rev.* **105**, 2811–2827 (2005)
35. Schiemann, M., Vorobiev, N., Scherer, V.: Stereoscopic pyrometer for char combustion characterization. *Appl. Opt.* **54**(5), 1097–108 (2015)
36. Schmidt, S., Ilic, C., Schulz, V., Gauger, N.R.: Three-dimensional large-scale aerodynamic shape optimization based on shape calculus. *AIAA J* **51**(11), 2615–2627 (2013)
37. Spalding, D.: Combustion of fuel particles. *Fuel* **30** (2016)
38. Stauch, R., Maas, U.: Transient detailed numerical simulation of the combustion of carbon particles. *Int. J Heat Mass Trans.* **52**(19), 4584–91 (2009)

-
39. Tirado, C., Jiménez, S., Ballester, J.: Gasification of a pulverized sub-bituminous coal in co₂ at atmospheric pressure in an entrained flow reactor. *Combust. Flame* **159**, 385–395 (2012)
 40. Tirado, C., Jiménez, S., Johansson, R., Ballester, J.: Comparative study of four alternative models for co oxidation around a burning coal char particles. *Combust. Flame* **161**, 1085–1095 (2014)
 41. Wei, M., Freund, J.: A noise-controlled free shear flow. *J Fluid Mech.* **546**, 123 (2005)
 42. Zhang, H., Sandu, A.: Fatode: A library for forward, adjoint, and tangent linear integration of odes. *SIAM J Sci. Comput.* **36** (2014)